Supporting information

WO_3 Nanorods/Graphene Nanocomposites for High-Efficiency Visible-Light-Driven Photocatalysis and NO_2 Gas Sensing

Xiaoqiang An,[a] Jimmy C. Yu,[*a] Yu Wang,[b] Yongming Hu,[b] Xuelian Yu[c] and Guangjin Zhang[c]
[a] Department of Chemistry and Institute of Environment, Energy and Sustainability, The Chinese University of Hong Kong, Shatin, New Territories, Hong Kong, China
E-mail: jimyu@cuhk.edu.hk
[b] Department of Applied Physics and Materials Research Center, The Hong Kong Polytechnic University, Hong Kong SAR, PR China
[c] Institute of Process Engineering, Chinese Academy of Science, Beijing 100190, People's Republic of China

Fabrication of graphene oxide (GO)

GO was synthesized by a modified Hummers' method. In detail, 2 g of graphite was pre-oxidized before subjected oxidation. The pre-oxidized graphite was then added to a mixture of 120 mL of concentrated H_2SO_4 and 30 mL HNO_3 in an ice-water bath. 15 g $KMnO_4$ was added while the temperature was kept below 20 °C. After stirring for 3 days at 35 °C, the mixture was diluted with 1 L of DI water and stirred at 98 °C for 0.5 hour. Shortly after the further dilution with 1 L of DI water, 20 mL of 35% H_2O_2 was added to end the reaction. Subsequently, the mixture was filtered and washed with 1: 10 HCl aqueous solution and DI water in turn. The collected precipitate was dispersed in 150 mL of water and sonicated for 30 min. After centrifuging at 5000 r/min for 5 min, a brown homogeneous supernatant of graphene oxide was obtained. The final concentration of GO was determined to be 4 mg/mL.

Thermogravimetric analysis (TGA)

TGA is an effective analytical technique to evaluate the ratio of graphene and WO_3. From Fig. s1, WO_3 nanorods/graphene composites shows remarkable weight loss from room temperature to 280 °C, which is due to the loss of water. The mass loss from 400 to 550 °C is ascribed to the decomposition of oxygen-containing group and carbon oxidation from graphene. Based on the total weight loss of WO_3/graphene composites, the weight ratio of graphene in the composites is determined to be 3.5 wt%.

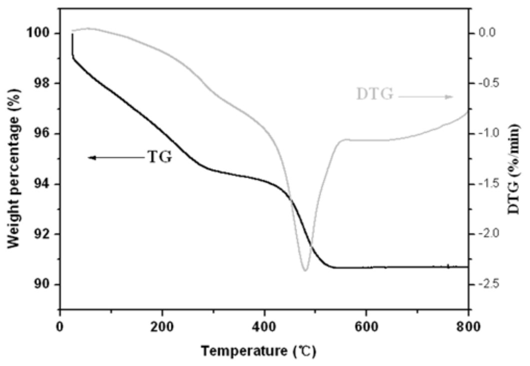

Fig. s1 TGA curves of WO_3 nanorods/graphene composites.

Fourier-Transform Infrared (FTIR) Analysis

The structures of WO_3 nanorods, GO and WO_3 nanorods/graphene composites are characterized by FTIR spectra, which are shown in Fig. s2. For the spectrum of WO_3 nanorods/graphene, the characteristic absorption bands of the C=O stretching vibration (1735 cm^{-1}) and the C-O (alkoxy) stretching peak (1080 cm^{-1}) disappear after the hydrothermal reduction of GO, indicating the decomposition of the oxygen-containing functional groups. Besides, the increased band at 1633 cm^{-1} can be assigned to the skeletal vibration of graphene sheets. These changes indicate the formation of WO_3 nanorods/graphene composites. The interactions between residual carboxyl groups of graphene and WO_3 nanorods are also confirmed by the obvious asymmetric COO– stretching bonds around 1598 cm^{-1}.[1]

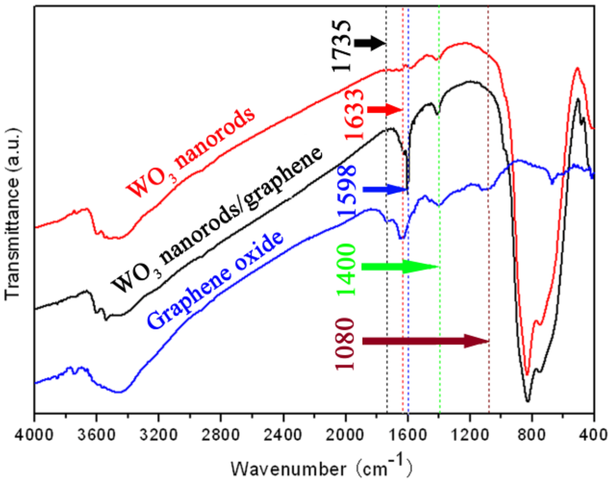

Fig. s2 FTIR spectra of GO, WO_3 nanorods and WO_3 nanorods/graphene composites.

Raman Analysis

Raman scattering is sensitive to the microstructure of nanocrystalline materials, so it is employed to determine the structure of WO_3 nanorods/graphene composites. As shown in Fig. s3a, the peaks located at 245 cm^{-1}, 325 cm^{-1}, 806 cm^{-1} and 924 cm^{-1} are consistent with the fundamental modes of crystalline h-WO_3. These bands are respectively ascribed to the O-W-O stretching modes of the bridging oxygen (245 cm^{-1} and 325 cm^{-1}), the O-W-O bending modes (806 cm^{-1}) and the stretching mode of the terminal W=O (924 cm^{-1}).[2] The characteristic scatterings of graphene in the composites are observed at 1363 cm^{-1} (D band), 1606 cm^{-1} (G band) and 2620 cm^{-1} (2D band). In another experiment, graphene was also directly fabricated after a similar hydrothermal reduction of GO. Compared with graphene, the G band in WO_3 nanorods/graphene composites shift to the higher wavenumber in Fig. s3b. This shift might be caused by the presence of isolated double bonds separated by functional groups on the carbon network.[3] In addition, the 2D band around 2625 cm^{-1} is the second order of zone-boundary phonons and the S3 peak near 2930 cm^{-1} is a result of lattice disorders referred as to the combination of the G and D peaks. For the spectrum of WO_3 nanorods/graphene, the 2D band locates at lower wavenumber, indicating the aggregation of graphene sheet into multilayered structure can be avoided in the presence of WO_3 nanorods.[4]

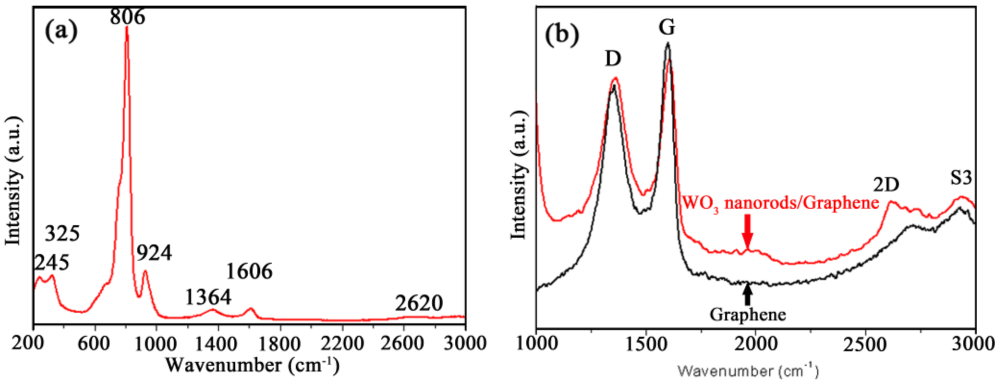

Fig. s3 (a) Raman spectra of WO_3 nanorods/graphene composites; (b) Raman spectra of graphene and WO_3 nanorods/graphene composites from 1000-3000 cm^{-1}.

N_2 adsorption–desorption isotherm

Fig. s4a shows the N_2 adsorption–desorption isotherms of pure WO_3 nanorods and WO_3 nanorods/graphene composites. Typically, both samples show isotherms of type IV, indicating the presence of mesopores.[5] The nonlimiting adsorption at high P/P_0 is characteristic of a Type H3 loop. The BET analysis reveals that the WO_3 nanorods/graphene has a surface area of 34.8 m^2/g, which is higher than 29.3 m^2/g of the neat WO_3. As the porosity and special surface affinity show significant influence on the photodegradation of dye, the remaining RhB 6G in solution after the adsorption equilibrium for 12 hours over WO_3/graphene composites is studies in Fig. s4b. It is observed that all the WO_3/graphene composites exhibit enhanced adsorptivity of RhB 6G. For WO_3 nanorods/3.5 wt% graphene, the calculated ratio of dye capture is 28% higher than the WO_3 nanorods.

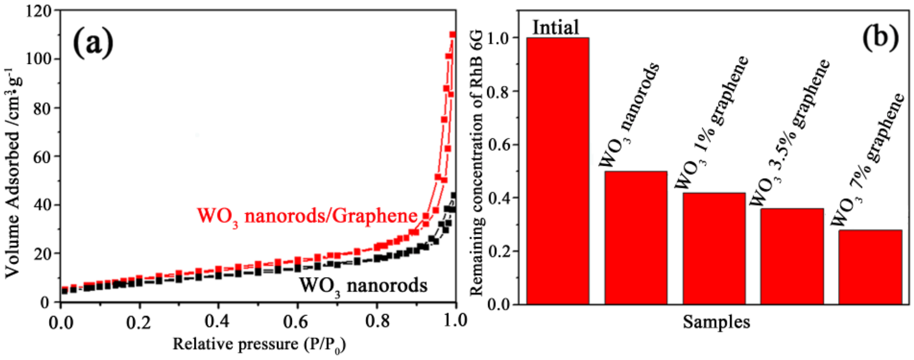

Fig. s4 (a) Nitrogen isotherm adsorption-desorption curves of WO_3 nanorods and WO_3 nanorods/graphene composites; (b) Bar plot showing the remaining RhB 6G in solution after the adsorption equilibrium in the dark for 12 hours over WO_3 nanorods and WO_3 nanorods/graphene composites.

UV-vis absorption

The optical properties of the samples are characterized by UV-vis spectroscopy in Fig. s5. The addition of different amount of graphene shows great influence on the light absorption of WO_3 nanorods, with significant enhanced absorption intensity in the visible light region. The band located at around 250 nm is ascribed to the π-π□ transition of graphene. The charge transfer from WO_3 to graphene is easily deduced from the red shift of this characteristic band.[6]

Photoelectrochemical test

For the photoelectrochemical measurement, platinum wire was used as the counter electrode and the Ag/AgCl electrode as the reference electrode. The electrolyte was 1M KCl solution degassed with Ar. The illumination source was a 500W xenon lamp with a cutoff filter (λ>420nm). The photocurrent measurement was carried out with an electrochemical workstation system (Parstat 2273, Princeton Applied Research).

The photoelectrochemical behaviour of the WO_3 nanorods and WO_3 nanorods/graphene composites under visible-light irradiation is shown in Figure s5b. Obviously, the photocurrent of WO_3/graphene composites to each switch-on and switch-off event is improved significantly. This enhanced photocurrent confirms a more efficient separation of the photoexcited electron-hole pairs as compared with pure WO_3.

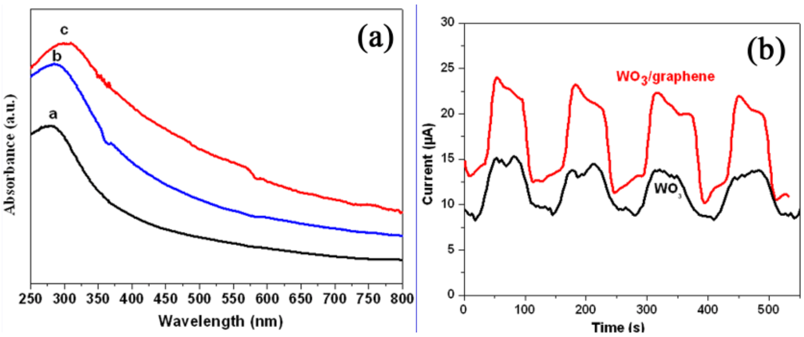

Fig. s5 UV-vis spectra of WO_3 nanords/graphene composites. (a: WO_3 nanorods; b: WO_3 nanorods/1 wt% graphene; c: WO_3 nanorods/3.5 wt% graphene composites); (b) The photoresponse of WO_3 and WO_3/graphene composites to visible light irradiation.

Photoluminescence spectra and spectral changes of RhB 6G during photocatalytic reaction

The efficient charge separation and transfer are crucial for the enhanced photocatalytic activity of WO_3/graphene composites. The PL spectra of WO_3 nanorods and WO_3 nanorods/graphene composites with an excitation wavelength of 325 nm are shown in Fig. s6. As-prepared WO_3 nanorods show emission peaks at 440 nm, 466 nm and 540 nm in the visible light region, due to the electronic transition of WO_3. While after their combination with graphene, the intensity of emission peak is significantly quenched. It suggests an additional pathway for the electron transfer, from the conduction band of excited WO_3 to graphene sheets.[7] The role of graphene as an acceptor of the generated electrons can efficiently suppress the charge recombination, which leads to more reactive species for the improved photocatalytic reactions.[8]

RhB 6G can be degraded by both photocatalytic de-methylation and photosensitized de-ethylation. An absorption blue shift is often used to confirm the photosensitized process.[9] Figure s6b and Figure s6c show the temporal evolution of the spectral changes of RhB 6G mediated by WO_3/graphene composites and WO_3 nanorods. It can be seen that after 3 hours of irradiation, the blue shift of the absorption peak at 525 nm is very small (no more than 5 nm after 3 hours). It indicates that the degradation of the Rhodamine dye on WO_3/graphene is primarily caused by a photocatalytic process. For comparison, we also studied the degradation of RhB 6G over pure TiO_2. It is known that photosensitized degradation play an important role in systems involving TiO_2 nanoparticles. A much larger peak shift (23 nm after 1.5 hour) is observed in Figure s6d, suggesting a predominantly de-ethylation reaction for TiO_2 photocatalyst.[10] The different reaction pathways for degradation over WO_3/graphene and TiO_2 can be explained by the different secondary chemical events that occur after visible-light-induced electron injection.[11]

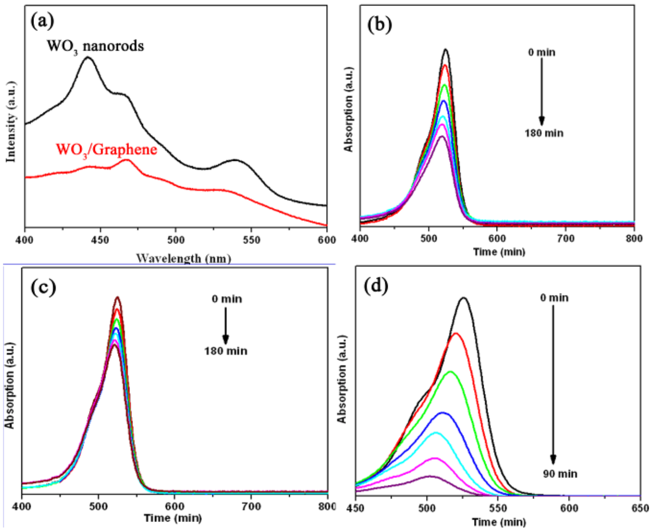

Fig. s6 (a) Photoluminescence spectra of WO_3 nanorods and WO_3 nanorods/graphene composites with an excitation wavelength of 325 nm. (b-d) Time-dependent absorption spectra of RhB 6G under visible-light. (b) WO_3/graphene composites; (c) WO_3 nanorods; (d) TiO_2 nanoparticles.

Composites based on the other carbonaceous materials and the stability of photocatalysts

The photocatalytic property of WO_3/graphene composites is compared to the WO_3/carbon nanotubes and WO_3/carbon black composites. As shown in Figure s7a, WO_3/(3.5%) carbon nanotubes composites show poor photocatalytic performance. The deteriorated photocatalytic activity can be ascribed to the poor interfacial contact between 1-D nanorods and 1-D nanotubes. The elimination efficiency of RhB 6G with WO_3/carbon black is slightly lower than that of WO_3/graphene composites, indicating the necessity of WO_3-carbon composites for improving the photocatalytic activity of WO_3.

To investigate to stability of photocatalysts, the photodegradation of RhB 6G was repeated for four cycles, each for 180 min. After each cycle, WO_3/graphene was filtrated and washed thoroughly with water and ethanol. As shown in Figure s7b, there is no significant decrease in photodegradation rate during the four cycles, indicating the good stability of the WO_3/graphene photocatalyst.

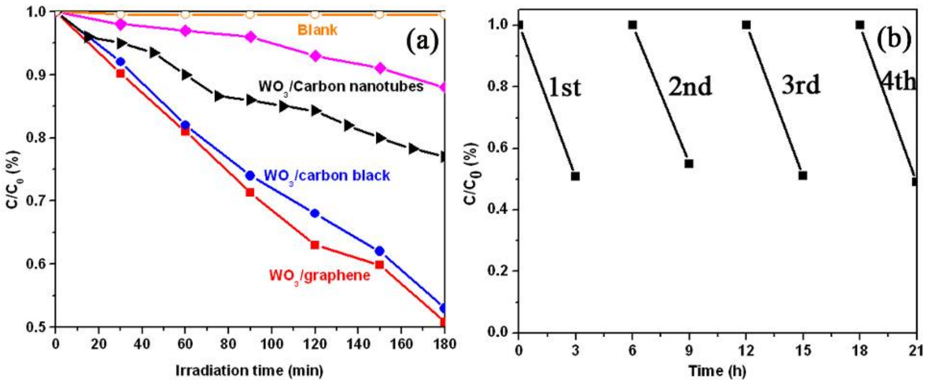

Figure s7 (a) Photodegradation of RhB 6G over WO_3 and several types of WO_3-carbon composites. (b) Repeating experiment results of photodegradation of RhB 6G over WO_3/graphene composites.

Calibration curves of gas sensing property of sensors

Figure s8 shows the calibration curve of WO_3 and WO_3/graphene composites for NO_2 detection. The detecting limit ($3S_b/k$, S_b is standard deviation, k is slope of the curve) is 3.17 ppb for the sensor of WO_3/graphene composites, indicating its good sensitivity. It also shows a wide linear range between 25 ppb and1000 ppb, with a relative standard deviation (RSD) of 12%. As for the sensor made of WO_3 nanorods, the linear range is only between 25 ppb and 500 ppb.

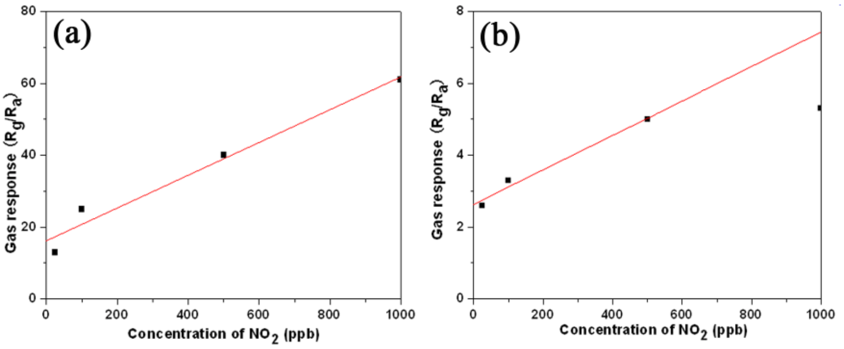

Figure s8 Calibration curves for WO_3/graphene composites (a) and WO_3 (b) for NO_2 detection.

References

1 J. Su, M. Cao, L. Ren and C. Hu, *J. Phys. Chem. C* 2011, **115**, 14469.

2 J. Ha, P. Muralidharan and D. Kim, *J. Alloys Compd*. 2009, **475**, 446.

3 J. Shen, B. Yan, M. Shi, H. Ma, N. Li and M. Ye, *J. Mater. Chem*. 2011, **21**, 3415

4 M. Dresselhaus, A. Jorio, M. Hofmann, G. Dresselhaus and R. Saito, *Nano Lett*. 2010, **10**, 751.

5 N. Li , G. Liu, C. Zhen, F. Li, L. Zhang and H. Cheng, *Adv. Func. Mater*. 2011, **21**, 1717.

6 B. Choi, W. Hong, Y. Jung and H. Park, *Chem. Commun*. 2011, **47**, 10293.

7 J. Liu, H. Bai, Y. Wang, Z. Liu, X. Zhang and D. Sun, *Adv. Funct. Mater.* 2010, **20**, 4175.

8 K. Manga, Y. Zhou, Y. Yan and K. Loh, *Adv. Funct. Mater*. 2009, **19**, 3638.

9 M. Feng, M. Zhang, J. Song, X. Li and S. Yu, *ACS Nano*, 2011, **5**, 6726.

10 J. Zhang, Z. Xiong and X. S. Zhao, *J. Mater. Chem*., 2011, **21**, 3634.

11 C. Chen, W. Zhao, P. Lei, J. Zhao and N. Serpone, *Chem. Eur. J*. 2004, **10**, 1956.